Hyperbolic Secant LMS Algorithm to Enhance Performance of a Three-Phase Single-Stage Grid Connected PV System

Markala Karthik
Dept. of Electrical Engineering
NIT Rourkela
Odisha, India
markalakarthikreddy@gmail.com

Venkata Ramana Naik N
Dept. of Electrical Engineering
NIT Rourkela
Odisha, India
nenavathv@nitrkl.ac.in

Anup Kumar Panda
Dept. of Electrical Engineering
NIT Rourkela
Odisha, India
akpanda@nitrkl.ac.in

***Abstract*— Hyperbolic secant cost function based least mean square (HSLMS) algorithm is presented in this article to improve the performance of a three-phase single-stage grid-connected photovoltaic system (GCPVS) to improve its overall performance under adverse circumstances. The nonlinear loads at the distribution end pose a number of power quality challenges for the integration of distributed energy resources like solar photovoltaic (PV) energy. Nonlinearity, disturbances, and unbalanced loads cause these uncertainties. The key objective of this article is to operate the GCPVS to extract maximum PV power and solves the current related PQ problems. The characteristics of the hyperbolic secant cost function are employed to generate sinusoidal grid reference currents for harmonics mitigation, zero reactive power burden on the distribution grid, and to achieve unity power factor (UPF) mode of operation. The presented control structure is simulated in MATLAB/Simulink for analyzing the behavior of GCPVS during uncertain conditions.**

Keywords—Hyperbolic Secant Cost Function, Least Mean Square (LMS), Photovoltaic, Power Quality.

I. INTRODUCTION

Due to the continuous use of fossil fuels for the generation of electrical energy for decades, environmental concerns are being at the top priority level. Distributed generation by renewable energy sources (RES) is becoming popular which can reduce the environmental pollution effects to some extent and can reduce the long power transmission losses by supplying power to consumers loads locally. Solar photovoltaic (PV) farms are growing popular and solar energy is one among the distributed energy resources (DERs). PV farms has the advantages of low running cost, control over energy, eco-friendly, available in abundant, and noise-free can produce energy at bigger scale, and many more. On the other side the technology for solar cells manufacturing is growing at a faster rate for efficient utilization of PV power. As the distribution grid is generally of three-phase, the extracted PV power by the PV farms is to be integrated to the distribution grid for effective power management, thereby utilizing the grid as a source or a sink of power. The grid-connected PV system (GCPVS) can also serve the function of distribution static compensator when PV power is absent.

The GCPVS can be designed to have dc-dc converters or without. If it is designed with dc-dc converter in the form of double stage, the requirement of solid-state switches, cost, and power loss increases. However, the complexity of controlling converters switches is also high. Rather GCPVS is designed in the form of a single stage without having a dc-dc converter to overcome the demerits of a double-stage configuration.

The literature provides different types of control algorithms for operating GCPVS both in the time domain and in the frequency domain [1]. However, the frequency domain algorithms are complex to implement [2]. The time domain algorithms are derived based on instantaneous p-q and synchronous rotating frame theories which utilize transformations, and phase-locked loops (PLLs) [3, 4] increasing again the complexity of algorithms. In context to these algorithms, the weights updating-based adaptive filtering algorithms are popular in signal processing fields applications such as system identification and array beamforming. The most commonly used adaptive filtering algorithm is least mean square (LMS) [5] due to its simplicity, and ease of implementation. As LMS is not offering better performance for GCPVS in adverse conditions at the distribution grid, many variant algorithms of LMS [6], least mean fourth (LMF) family [7], and others were developed in the literature; considering variable step size [8, 9], different cost functions framework [10, 11], convex combination [12], and combined step size [13]. The complexity of all these algorithms is substantially high due to higher number of multiplications, additions, divisions, and other mathematical functions involved. This article is presenting a modified LMS algorithm [14] based on the hyperbolic secant cost function (HSLMS) which improves the transient behavior of the system by utilizing the characteristics of the hyperbolic secant cost function, and this algorithm is very simple to implement.

There are five sections in the article. The GCPVS configuration is presented in section II. In section III, the proposed HSLMS algorithm for GCPVS is elaborated in detail. Section IV reports the results of GCPVS using MATLAB/Simulink software. Section V presents the conclusion of the article.

II. SYSTEM CONFIGURATION

The GCPVS configuration is shown in Fig. 1. The PV array generated power is transferred to the local loads connected at PCC and to the grid after conversion from DC to AC power using a voltage source converter (VSC) having a DC-bus capacitor (C_{dc}). The VSC is including three legs with six IGBT switches to form a two-level inverter. The required gate pulses for VSC are generated by using the proposed HSLMS algorithm. The local loads are realized in the form of nonlinear loads as most of the modern power system loads are being designed with power electronics

components. The load is being considered as an uncontrolled bridge rectifier feeding power to R-L load. Ripple filters and interfacing inductors are employed to mitigate high-frequency harmonic signals. The GCPVS parameters designed [15] and utilized in the simulation are given in Table I along with mathematical formula.

III. HSLMS ALGORITHM FOR GCPVS

The weight updating equation in HSLMS algorithm is derived by considering the hyperbolic secant cost function (1)

$$J(e(i)) = \text{sech}\{e^2(i)\} - 0.5\delta e^2(i) \tag{1}$$

where, *'δ'* is a positive constant and sech{.} is a hyperbolic secant function, and '*e*(*i*)' is an adaptive error. The weight updation relation derived using the HSLMS algorithm and is utilized in the control structure shown in Fig. 2 illustrated further.

From sensed line voltages at PCC, phase voltages (v_{sryb}) and inphase and quadrature voltage unit templates (u_{pryb}, u_{qryb}) are calculated [16] using (2) –(5)

$$\left.\begin{aligned} v_{sr} &= \left(2v_{sry} + v_{syb}\right)/3 \\ v_{sy} &= \left(-v_{sry} + v_{syb}\right)/3 \\ v_{sb} &= \left(-2v_{syb} - v_{sry}\right)/3 \end{aligned}\right\} \tag{2}$$

$$V_{st} = \sqrt{\frac{2}{3}(v_{sr}^2 + v_{sy}^2 + v_{sb}^2)} \tag{3}$$

$$u_{pr} = \frac{v_{sr}}{V_{st}}; u_{py} = \frac{v_{sy}}{V_{st}}; u_{pb} = \frac{v_{sb}}{V_{st}} \tag{4}$$

$$\left.\begin{aligned} u_{qr} &= \frac{u_{pb} - u_{py}}{\sqrt{3}} \\ u_{qy} &= \frac{\sqrt{3}u_{pr}}{2} + \frac{(u_{py} - u_{pb})}{2\sqrt{3}} \\ u_{qb} &= \frac{(u_{py} - u_{pb})}{2\sqrt{3}} - \frac{\sqrt{3}u_{pr}}{2} \end{aligned}\right\} \tag{5}$$

The GCPVS can be operated to either in unity power factor mode (UPF) or voltage regulation mode. In UPF mode, the grid currents maintain UPF with respective grid voltages where as in voltage regulation mode, the PCC voltage drop can be compensated. The modes of operation are not possible at a time.

The sinusoidal currents can be injected to the grid from PV using the estimated fundamental active weight from the harmonics polluted load currents. In voltage regulation mode, the reactive weight components estimated from the load current are included in the control structure whereas in UPF mode, these components are set to zero. The updated filter weights give the fundamental active and reactive weight components by utilizing polluted load current and unit voltage templates of three phases separately as depicted in Fig. 2. These filter weights are updated for three phases as per the HSLMS algorithm using from (6) to (23). Active weight components (w_{pr}, w_{py}, w_{pb}) are obtained as

$$w_{pr}(i+1) = w_{pr}(i) + \mu f(e_{pr}(i))u_{pr} \tag{6}$$

$$\text{where, } f(e_{pr}(i)) = \left\{\frac{2\sinh\{e_{pr}^2(i)\}}{\left[\cosh\{e_{pr}^2(i)\}\right]^2} + \delta\right\} e_{pr}(i) \tag{7}$$

$$e_{pr}(i) = i_{Lr} - w_{pr}u_{pr} \tag{8}$$

$$w_{py}(i+1) = w_{py}(i) + \mu f(e_{py}(i))u_{py} \tag{9}$$

$$\text{where, } f(e_{py}(i)) = \left\{\frac{2\sinh\{e_{py}^2(i)\}}{\left[\cosh\{e_{py}^2(i)\}\right]^2} + \delta\right\} e_{py}(i) \tag{10}$$

$$e_{py}(i) = i_{Ly} - w_{py}u_{py} \tag{11}$$

$$w_{pb}(i+1) = w_{pb}(i) + \mu f(e_{pb}(i))u_{pb} \tag{12}$$

$$\text{where, } f(e_{pb}(i)) = \left\{\frac{2\sinh\{e_{pb}^2(i)\}}{\left[\cosh\{e_{pb}^2(i)\}\right]^2} + \delta\right\} e_{pb}(i) \tag{13}$$

$$e_{pb}(i) = i_{Lb} - w_{pb}u_{pb} \tag{14}$$

Similarly, the reactive weight components for phases *r*, *y*, *b* (w_{qr}, w_{qy}, w_{qb}) are updated as

$$w_{qr}(i+1) = w_{qr}(i) + \mu f(e_{qr}(i))u_{qr} \tag{15}$$

$$\text{where, } f(e_{qr}(i)) = \left\{\frac{2\sinh\{e_{qr}^2(i)\}}{\left[\cosh\{e_{qr}^2(i)\}\right]^2} + \delta\right\} e_{qr}(i) \tag{16}$$

$$e_{qr}(i) = i_{Lr} - w_{qr}u_{qr} \tag{17}$$

$$w_{qy}(i+1) = w_{qy}(i) + \mu f(e_{qy}(i))u_{qy} \tag{18}$$

$$\text{where, } f(e_{qy}(i)) = \left\{\frac{2\sinh\{e_{qy}^2(i)\}}{\left[\cosh\{e_{qy}^2(i)\}\right]^2} + \delta\right\} e_{qy}(i) \tag{19}$$

$$e_{qy}(i) = i_{Ly} - w_{qy}u_{qy} \tag{20}$$

$$w_{qb}(i+1) = w_{qb}(i) + \mu f(e_{qb}(i))u_{qb} \tag{21}$$

$$\text{where, } f(e_{qb}(i)) = \left\{\frac{2\sinh\{e_{qb}^2(i)\}}{\left[\cosh\{e_{qb}^2(i)\}\right]^2} + \delta\right\} e_{qb}(i) \tag{22}$$

$$e_{qb}(i) = i_{Lb} - w_{qb}u_{qb} \tag{23}$$

To have a balance among three-phase load currents, the average of the weight components is considered as

$$w_{pav} = (w_{pr} + w_{py} + w_{pb})/3 \tag{24}$$

$$w_{qav} = (w_{qr} + w_{qy} + w_{qb})/3 \tag{25}$$

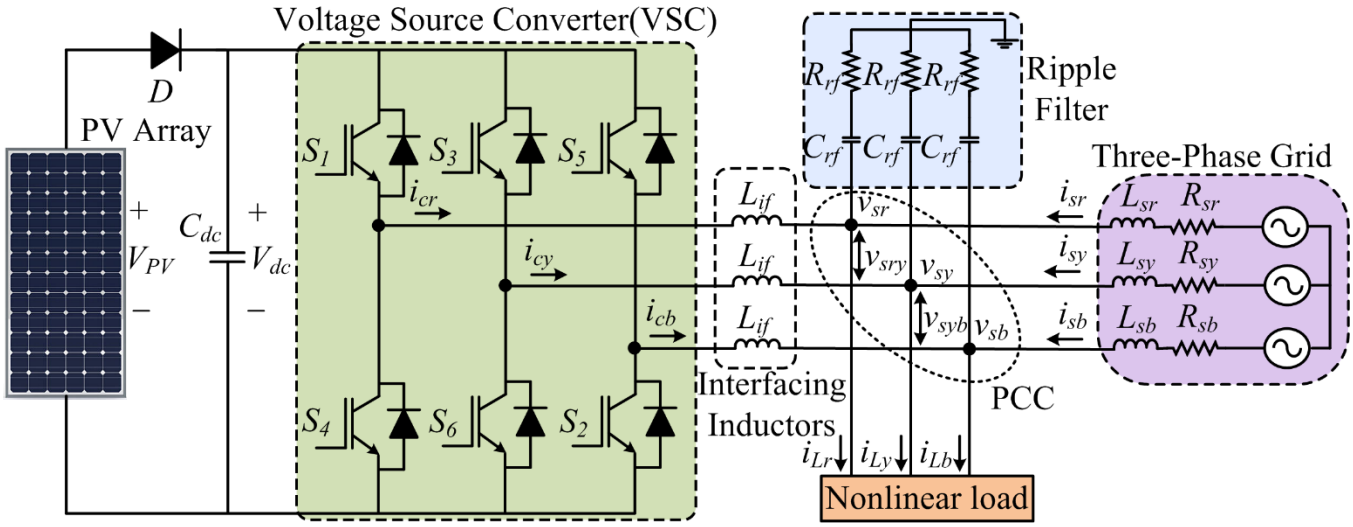

Fig. 1. Three-phase single-stage GCPVS configuration

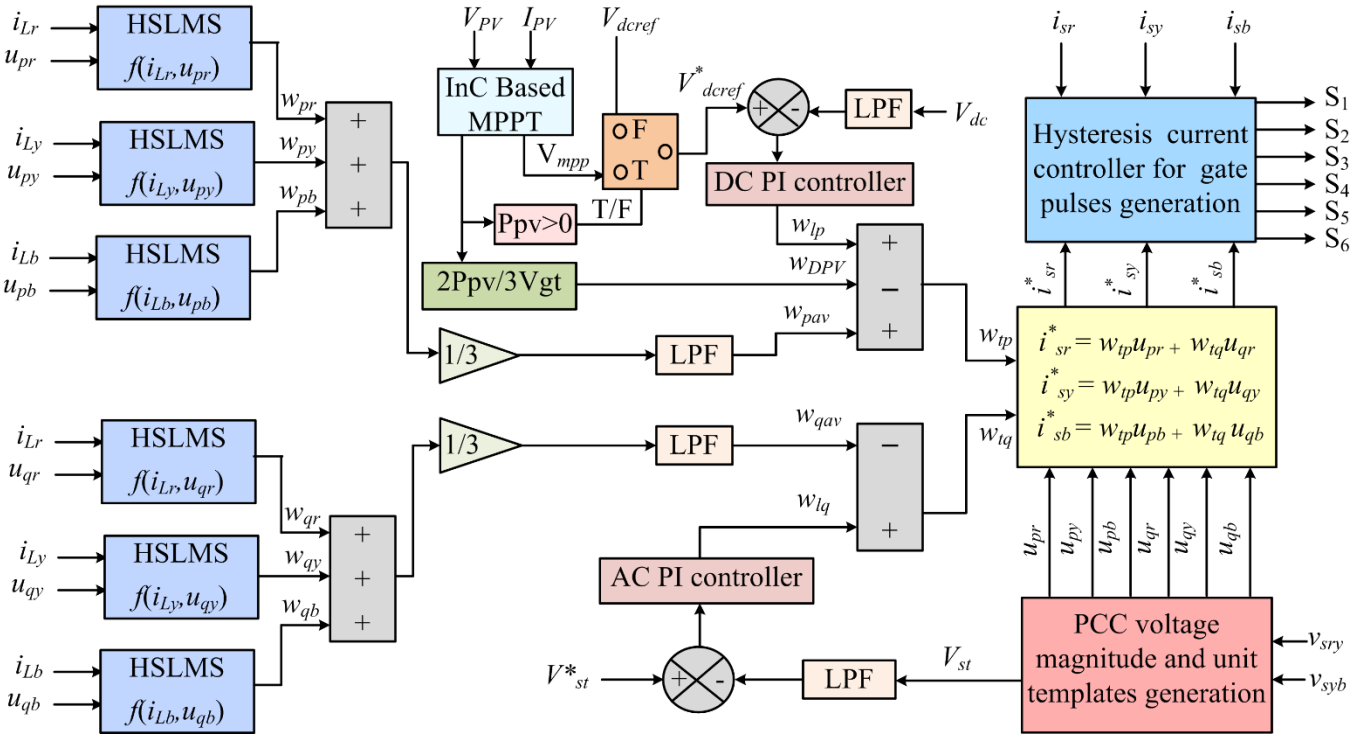

Fig.2. HSLMS algorithm-based control structure for GCPVS

The DC-bus voltage (V_{dc}) is maintained equal to V_{mpp} (PV array voltage at maximum power point condition) to utilize the maximum power produced by PV array in the system during sun light availability using a DC PI controller. This DC PI controller output is considered as an active power loss component given by

$$w_{lp} = K_{p1} \times e_{dc}(i) + K_{I1} \sum_{i=0}^{t} e_{dc}(i) \tag{26}$$

where, $e_{dc}(i) = V^*_{dcref} - V_{dc}$ (27)

Here, $V^*_{dcref} = V_{mpp}$ when $P_{PV} > 0$

$V^*_{dcref} = V_{dcref}$ when $P_{PV} = 0$

During non-availability of sun light, V_{dc} has to be maintained at DC-bus reference voltage (V_{dcref}) which is calculated as $\left(2\sqrt{2}v_{s(L-L)}/\sqrt{3}m\right)$. Here '$m$' is a modulation index considered as '1'. During the sun light availability 'V_{mpp}' is obtained by implementing incremental conductance based maximum power point technique (InC-based MPPT).

The reactive loss component responsible to maintain PCC voltage magnitude constant in case of voltage drop due to local loads is obtained as an output of AC PI controller which is expressed as

$$w_{lq} = K_{p2} \times e_{ac}(i) + K_{I2} \sum_{i=0}^{t} e_{ac}(i) \tag{28}$$

where, $e_{ac}(i) = V^*_{st} - V_{st}$ (29)

Here, V^*_{st} is the required PCC voltage magnitude and V_{st} is the measured PCC voltage magnitude. For the considered PCC voltage of 415 V (line to line rms), $V^*_{st} = 340$ V.

The sinusoidal reference currents desired to be injected/drawn to/from the grid can be obtained as

$$i_{sr}^{*} = w_{tp}u_{pr} + w_{tq}u_{qr} \quad (30)$$

$$i_{sy}^{*} = w_{tp}u_{py} + w_{tq}u_{qy} \quad (31)$$

$$i_{sb}^{*} = w_{tp}u_{pb} + w_{tq}u_{qb} \quad (32)$$

where, $w_{tp} = w_{pav} + w_{lp} - w_{DPV}$ (33)

$$w_{tq} = w_{lq} - w_{qav} \quad (34)$$

Here the PV dynamic reflection weight component (w_{DPV}) is included in the total active weight component. 'w_{DPV}' is used to improve the dynamic performance of grid currents during the change in PV system parameters.

Now these reference currents and actual grid currents are subtracted from each other and this error is given to hysteresis current controller to get the gate pulses for the VSC.

IV. Resutls and Discussion

The performance of three-phase single-stage GCPVS with the proposed HSLMS algorithm is analysed by simulating in MATLAB/Simulink software.

A. Response of GCPVS with Unbalanced Nonlinear Load

The behavior of GCPVS with unbalanced nonlinear load is analyzed from Fig. 3. and Fig. 4. To create this situation, one phase of the connected nonlinear load is disconnected (Here it is phase '*b*'). Before unbalanced loading conditions, the HSLMS control algorithm is operating GCPVS to have balanced sinusoidal currents at the grid side (i_{sryb}). At the instant of phase '*b*' disconnection, due to less power consumption by the load, the grid currents start increasing and settle to the previous value once the load restores. During the load unbalance also, the grid is maintaining balanced currents because of the capability of the implemented control structure. From 0.25 s to 0.3 s, as load power (P_L) is reduced due to the removal of phase '*b*', the power injected to grid (P_g) from PV is increased. The grid is supplying zero reactive power (Q_g), and DC-bus voltage is always regulated to constant value. Fig. 4 shows adaptive active error estimated by HSLMS algorithm for phase '*r*'(e_{pr}) and different weight components involved in the control structure. It is observed that all the weight components adapt as per the change in load current except 'w_{DPV}', since it is not depending on the load.

B. Response of GCPVS with Change in Solar Irradiation

The behavior of GCPVS when it is subjected to variable solar irradiation is shown in Fig. 5. The solar irradiation (G) is changed to 700 W/m^2 from 1000 W/m^2 during 0.25 s to 0.3 s and brought back to 1000 W/m^2. When 'G' is decreased, as there is a reduction in P_{PV}, the magnitude of 'i_{sryb}' is reduced due to reduced power feeding to the grid from PV and constant power drawing from the load. 'w_{DPV}' is also reduced during reduced 'G' as it is proportional to P_{PV}. 'w_{pav}' is not changed as it is independent of 'G'. Resultantly, there is a variation in the total active weight component 'w_{tp}'.

TABLE I. GCPVS PARAMETERS

Sl. No.	System Parameters		
	Description	***Mathematical formula***	***Value***
1	PV array power at MPP	P_{mpp}	11 kW
2	PV array voltage at MPP	V_{mpp}	700 V
3	PV array current at MPP	I_{mpp}	15.74 A
4	Grid voltage, $v_{s(L-L)}$	-	415 V
5	Grid frequency, ω	$\omega = 2\pi f$ (f= 50 Hz)	314 rad/sec
6	DC-bus voltage, V_{dc}	$\geq \frac{2\sqrt{2}v_{s(L-L)}}{\sqrt{3}m}$ (m = 1)	700 V
7	DC-bus capacitance, C_{dc}	$\frac{P_{PV}/V_{dc}}{2\omega V_{dcrip}}$ (V_{dcrip}= 2 % of V_{dc})	2000 µF
8	Ripple filter components, R_{rf} and C_{rf}	Tuned [12]	5 Ω, 5µF
9	Switching frequency, f_{sw}	-	20 kHz
10	Interfacing inductor, L_{if}	$\frac{\sqrt{3}mV_{dc}}{12 \times a \times f_{sw} \times \Delta i}$ (a = overloading factor= 1.2, Δi = % ripple current of peak current =3 %)	9 mH

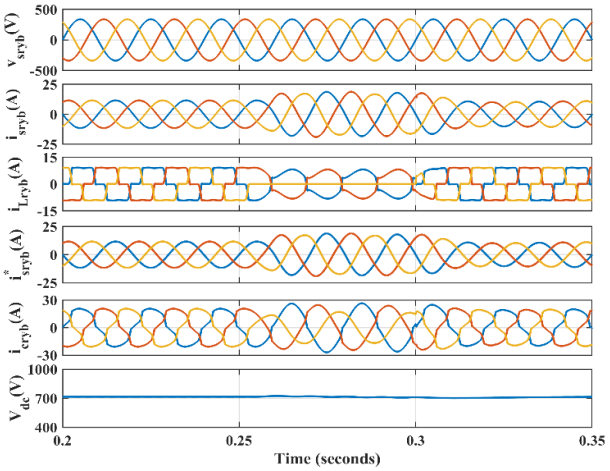

(a)

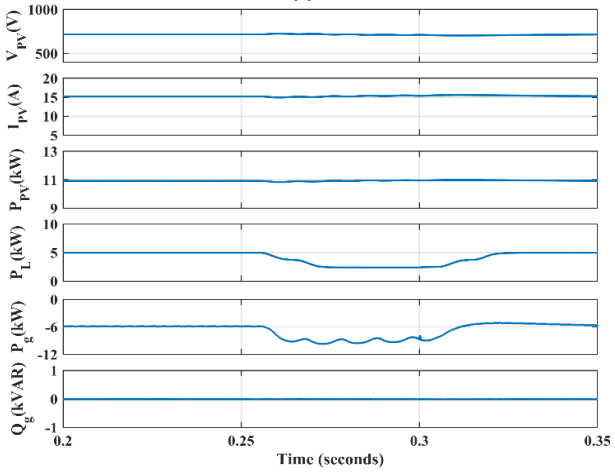

(b)

Fig. 3. (a)-(b): Response of GCPVS with unbalanced nonlinear load

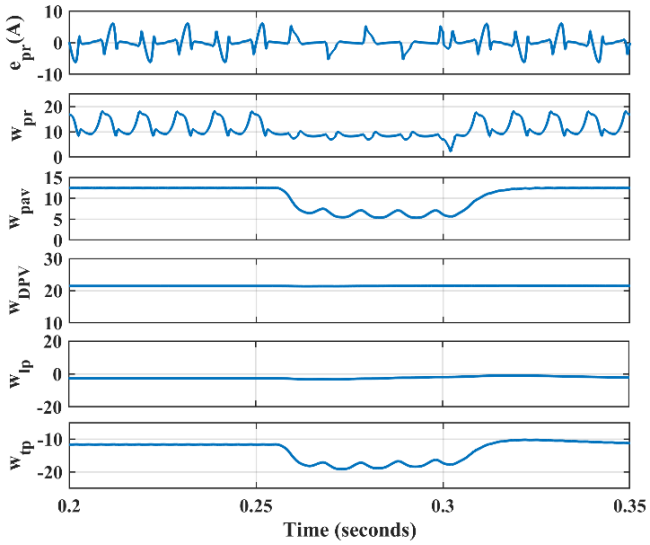

Fig. 4. Weight components involved in the control algorithm

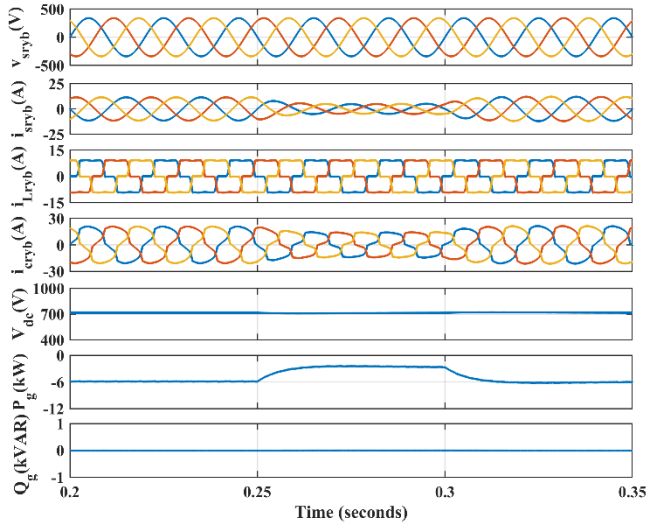

(a)

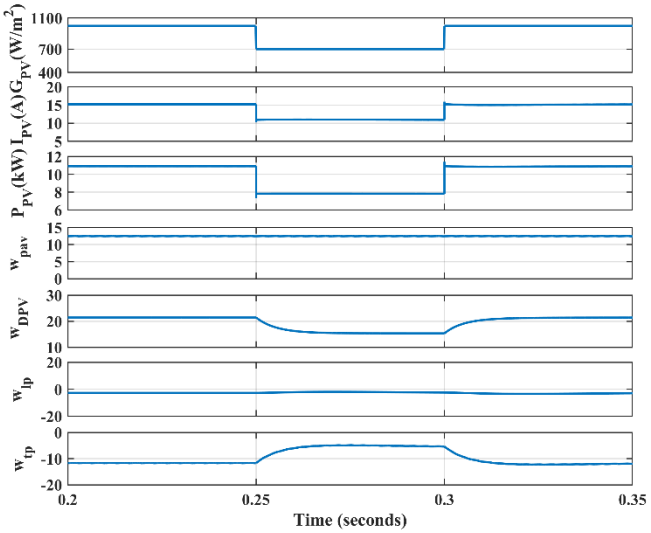

(b)

Fig. 5. (a)-(b): Response of GCPVS with change in solar irradiation

C. THD Measurement

The FFT spectrum for grid current and load current of phase '*r*' is shown in Fig. 6. The nonlinear load is rich in harmonics with a THD of 26.08 %. It is observed that as the harmonics component currents are supplied from VSC to the load, the THD of grid current is improved to 1.17 % which also satisfies the IEEE-519 standard [17].

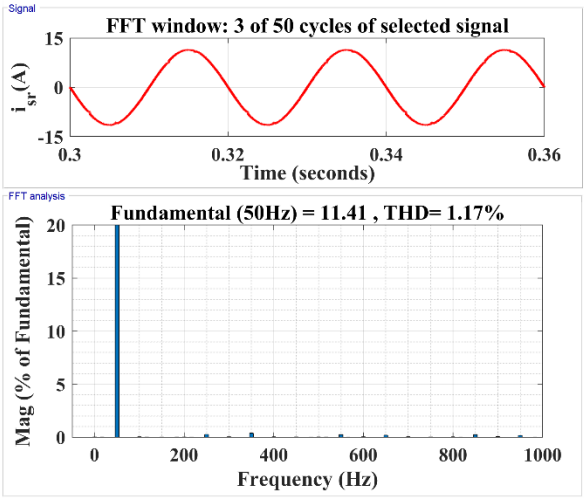

(a)

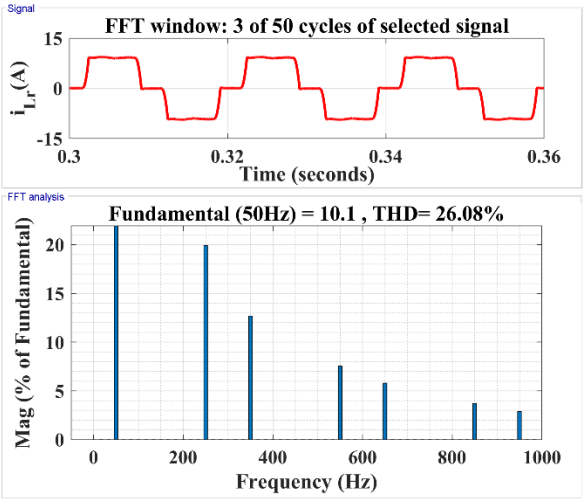

(b)

Fig. 6. FFT spectrum for (a) grid current, and (b) load current

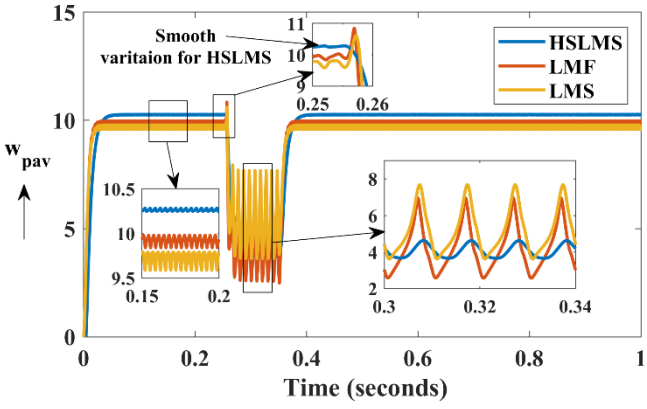

Fig. 7. 'w_{pav}' estimated by HSLMS, LMS and LMF algorithms

D. Comparison of HSLMS with LMS and LMF Algorithms

The performance of the proposed HSLMS algorithm is observed by analysing the weights estimation with that of other existing algorithms. Here, HSLMS algorithm is

compared with LMS and MF algorithms. For this purpose, an unbalance is created in the load from 0.25 s to 0.3 s, and the estimated 'w_{pav}' is compared as shown in Fig. 7. It is inferred, the oscillations during steady-state and dynamic loading conditions are less in magnitude for HSLMS algorithm than LMS and LMF. During change in loading conditions also, the weight estimation happened smoothly by HSLMS whereas LMS and LMF fails to have a smooth updation of weight components and the tracking speed is more in HSLMS algorithm.

V. Conclusion

The HSLMS algorithm-based control structure is presented for GCPVS. The characteristics of hyperbolic secant cost function utilized to improve the performance of GCPVS under adverse conditions by simulating GCPVS using MATLAB/Simulink software. GCPVS is operated in UPF mode while extracting maximum power from PV array, provided zero reactive power burden on the grid, and maintained balanced sinusoidal currents at the grid, while feeding nonlinear loads. The proposed HSLMS algorithm is compared with LMS and LMF algorithms. It is observed that HSLMS algorithm exhibits improved performance than LMS and LMF algorithms with increased convergence rate and less oscillations in magnitude while estimating weight components at steady state and dynamic conditions.

References

[1] F. Chishti, S. Murshid and B. Singh, "Grid Integration of Renewable Energy Generating System Using Nonlinear Harmonic Observer Under Nonideal Distribution System," *IEEE Trans. Ind. Appl.*, vol. 57, no. 6, pp. 5571-5581, Nov.-Dec. 2021.

[2] V. Gurugubelli, A. Ghosh, and A. K. Panda, "Comparison of Deadzone and Vanderpol Oscillator Controlled Voltage Source Inverters in Islanded Microgrid," in *Proc. IEEE 2nd Int. Conf. Smart Technol. Power, Energy Control*, 2021, pp. 1-6.

[3] K. Sridharan and B. Chitti Babu, "Accurate Phase Detection System Using Modified SGDFT-Based PLL for Three-Phase Grid-Interactive Power Converter During Interharmonic Conditions," *IEEE Trans. Instrum. Meas.*, vol. 71, p. 2022,Dec. 2021.

[4] V. Gurugubelli, A. Ghosh, and A. K. Panda, "A New Virtual Oscillator Control for Synchronization of Single-Phase Parallel Inverters in Islanded Microgrid," *Energy Sources, Part A: Recovery, Utilization, and Environmental Effects*, vol. 44, no. 4, Sep. 2022.

[5] X. B. Li, Y. Y. Fan, and K. Peng, "A variable step-size LMS adaptive filtering algorithm," *Proc. - 5th Int. Conf. Wirel. Commun. Netw. Mob. Comput. WiCOM 2009*, no. 2, pp. 1–4, Sep 2009.

[6] Singh, Sunaina, Seema Kewat, Bhim Singh, and Bijaya Ketan Panigrahi. "Adjoint least mean square control for solar photovoltaic array grid-connected energy generating system." *IET Energy Systems Integration*, vol. 4, no. 1, pp. 72-86, Mar. 2022.

[7] R. K. Agarwal, I. Hussain, and B. Singh, "LMF-based control algorithm for single stage three-phase grid integrated solar PV system," *IEEE Trans. Sustain. Energy*, vol. 7, no. 4, pp. 1379–1387, Oct. 2016.

[8] Pradhan S, Hussain I, Singh B, and Panigrahi BK, "Modified VSS-LMS-based adaptive control for improving the performance of a single-stage PV-integrated grid system," *IET Sci. Meas. Technol.*, vol. 11, no. 4, pp. 388–399, Jul. 2017.

[9] M. Karthik, V. Naik N, and A. K. Panda, "A Variable Step Size Logarithmic Hyperbolic Cosine Adaptive Filtering-Based Control Scheme for Grid-Tied PV-DSTATCOM to Enhance Power Quality," in *Proc. IEEE Int. Conf. Power Electron., Drives and Energy Syst.*, 2022, pp. 1–6.

[10] A. Verma and B. Singh, "CAPSA Based Control for Power Quality Correction in PV Array Integrated EVCS Operating in Standalone and Grid Connected Modes," *IEEE Trans. Ind. Appl.*, vol. 57, no. 2, pp. 1789-1800, Mar./Apr. 2021.

[11] M. Karthik, V. Naik N, and A. K. Panda, "A Robust Generalized Modified Blake–Zisserman Adaptive Filter-Based Control Scheme for Grid-Tied PV System to Improve Power Quality," in *Proc. IEEE Int. Conf. Power Electron., Drives and Energy Syst.*, 2022, pp. 1–6.

[12] N. Beniwal, I. Hussain, and B. Singh, "Implementation of the DSTATCOM with an i-PNLMS-Based Control Algorithm under Abnormal Grid Conditions," *IEEE Trans. Ind. Appl.*, vol. 54, no. 6, pp. 5640–5648, Nov. 2018.

[13] A. Kumar, N. Patel, N. Gupta, and V. Gupta, "L2 norm enabled adaptive LMS control for grid-connected photovoltaic converters," *IEEE Trans. Ind. Appl.*, vol. 58, no. 4, pp. 5328–5339, Jul./Aug. 2022.

[14] L. Lu, L. Chen, Z. Zheng, Y. Yu, and X. Yang, "Behavior of the LMS algorithm with hyperbolic secant cost," J. Franklin Inst., vol. 357, no. 3, pp. 1943–1960, Feb. 2020.

[15] S. B. Q. Naqvi, S. Kumar, and B. Singh, "Weak Grid Integration of a Single-Stage Solar Energy Conversion System with Power Quality Improvement Features under Varied Operating Conditions," *IEEE Trans. Ind. Appl.*, vol. 57, no. 2, pp. 1303–1313, Jan 2021.

[16] B. Singh, A. Chandra, and K. Al-Haddad, Power Quality Problems and Mitigating Techniques. London, U.K.: Wiley, 2015.

[17] IEEE Recommended Practice and Requirements for Harmonic Control in Electric Power Systems, IEEE Std 519-2014, 2014.